A coupled FEM-BEM algorithm for the inverse acoustic medium problem

S. Bagheri[1] S. C. Hawkins[2]

(Received 24 February 2015; revised 15 October 2015)

Abstract

We present a numerical scheme for reconstructing the refractive index of an inhomogeneous two dimensional medium using acoustic far field data. The numerical scheme is based only on the mild assumption that the inhomogeneous medium is contained in the unit disk, and does not require axis-symmetry or other similar restrictions. Reconstruction of the refractive index, without the assumption of axis-symmetry, is achieved using an expansion in the high order Logan–Shepp polynomials. The Logan–Shepp expansion coefficients of the refractive index are formulated as the solution of a nonlinear equation, which is solved using a regularised Newton-type solver. Nonlinear function evaluations, which involve solving a forward scattering problem, are performed using an efficient coupled finite-element/boundary element method,

which ensures that the radiation condition is incorporated exactly. The scheme is demonstrated by reconstructing challenging continuous and discontinous media from noisy far field data.

Contents

1 Introduction

The inverse medium problem arises when the material properties of an unknown medium are investigated by illuminating the medium with acoustic or electromagnetic waves and measuring the induced scattered field. We present an algorithm to reconstruct the material properties of the medium from measurements of the scattered field. Important applications include nondestructive testing, seismic inversion, and medical imaging. We consider the two dimensional acoustic inverse medium problem, which arises in electromagnetic and acoustic imaging of anisotropic media with a cylindrical structure.

In particular, we consider the interaction of an incident plane wave

$$u^{\mathrm{inc}}(x) = e^{\mathrm{i}kx\cdot\widehat{d}}\,, \tag{1}$$

with a two dimensional inhomogeneous medium described by the refractive index $m(x)$ for $x \in \mathbb{R}^2$. Here k is the incident wavenumber, and the unit vector $\widehat{d}$ is the plane wave direction.

We make the mild assumption that the inhomogeneity of the medium is contained in the unit disk B centred at the origin. Outside the unit disk the refractive index is constant, and we normalise so that

$$m(x) = 1\,, \quad x \notin B\,.$$

We refer to the inhomogeneous medium inside B as the scatterer.

Interaction of the incident field u^{inc} with the scatterer produces an induced field u. It is natural to split u into an exterior scattered field u^s and an interior field u^i. Thus

$$u(x) = \begin{cases} u^i(x)\,, & \text{for } x \in B\,, \\ u^s(x)\,, & \text{for } x \notin B\,. \end{cases} \tag{2}$$

In many applications, the quantity of interest is the far field of the scatterer,

$$u^\infty(\widehat{x}) = \lim_{|x|\to\infty} \sqrt{|x|}e^{-\mathrm{i}k|x|}u^s(x)\,, \tag{3}$$

where $\widehat{x} = x/|x|$.

The scattered field satisfies the homogeneous Helmholtz equation

$$\Delta u^s(x) + k^2 u^s(x) = 0\,, \quad x \in \mathbb{R}^2 \setminus B\,, \tag{4}$$

and the Sommerfeld radiation condition [4, Eqn. (3.85)]

$$\lim_{|x|\to\infty} \sqrt{|x|}\left(\frac{\partial u^s}{\partial x}(x) - \mathrm{i}ku^s(x)\right) = 0\,, \tag{5}$$

uniformly with respect to the direction $\widehat{\mathbf{x}}$. The interior field satisfies the inhomogeneous Helmholtz equation

$$\Delta u^i(\mathbf{x}) + k^2 m(\mathbf{x}) u^i(\mathbf{x}) = 0\,, \quad \mathbf{x} \in B\,. \tag{6}$$

The total field is

$$u^{tot}(\mathbf{x}) = \begin{cases} u^i(\mathbf{x})\,, & \text{for } \mathbf{x} \in B\,, \\ u^s(\mathbf{x}) + u^{inc}(\mathbf{x})\,, & \text{for } \mathbf{x} \notin B\,, \end{cases} \tag{7}$$

and continuity of the total field and its normal derivative across the boundary ∂B of B yields the transmission boundary conditions

$$u^s(\mathbf{x}) + u^{inc}(\mathbf{x}) = u^i(\mathbf{x})\,, \quad \text{for } \mathbf{x} \in \partial B\,, \tag{8}$$

$$\frac{\partial u^s}{\partial \mathbf{n}}(\mathbf{x}) + \frac{\partial u^{inc}}{\partial \mathbf{n}}(\mathbf{x}) = \frac{\partial u^i}{\partial \mathbf{n}}(\mathbf{x})\,, \quad \text{for } \mathbf{x} \in \partial B\,, \tag{9}$$

where $\mathbf{n}(\mathbf{x})$ denotes the unit outward normal to ∂B at $\mathbf{x}$.

For a given incident direction $\widehat{\mathbf{d}}$ and given refractive index $m(\mathbf{x})$, the *forward problem* is to compute the induced fields u^s and u^i that satisfy (4)–(9) and the corresponding far field. Section 2 describes the coupled finite and boundary element method (FEM-BEM) scheme for the forward scattering problem.

Our focus is on solving the corresponding *inverse problem*, that is, computing the refractive index m using given far field data. Our starting point is an efficient solver for the forward problem based on the coupled FEM-BEM scheme [12]. This scheme employs the flexibility of the finite element method for the bounded inhomogeneous medium in B, and the efficiency of the boundary element method for the unbounded homogeneous medium exterior to B. A particular advantage of this approach is that the radiation condition (5) is satisfied exactly.

A key feature of our algorithm, that allows us to avoid assumptions such as axis-symmetry of the refractive index, is the use of the Logan–Shepp polynomials [13] as a basis for the high order approximation of the refractive

index function $\mathfrak{m}$ inside B. These polynomials were recently used to compute high order approximations on the disk for various elliptic PDE problems [2].

Typically coarse scale features, such as the location and extent of inhomogeneities in the refractive index, are the key features of interest. We demonstrate in several examples that Logan–Shepp polynomials with degree of the order of ten are sufficient for reconstructing the key features of the refractive index $\mathfrak{m}$. Section 3 formulates the inverse problem as an ill-posed nonlinear equation, which we solve for the Logan–Shepp expansion coefficients using the Levenburg–Marquardt algorithm [8, 4, 11]. A consequence of the low polynomial degree is that the corresponding low dimensional discrete nonlinear problems are solved cheaply by assembling the Jacobian and using a direct solver.

The extensive literature on inverse scattering problems [4, and references therein] is predominantly focused on the problem of reconstructing the shape (or impedence) of impenetrable scatterers. The theory for the inverse medium problem is comparatively undeveloped, and uniqueness results do not sharply specify the type or quantity of data required [4, §10.2]. However, Newton-type methods were successfully applied to the inverse medium problem. In particular, for square (or cubic) domains the quasi-Newton method was applied to compute the tensor product Fourier coefficients of the refractive index [7, 5, 6]. For three dimensional spherical domains, the refractive index was represented using a tensor product of the spherical harmonics and splines [9, 10]. In the latter case, the scattering problem was reformulated using the Lippman–Schwinger volume integral equations, and the resulting nonlinear problem was solved using the Levenburg–Marquardt iteration. We are not aware of any other articles that use a coupled FEM-BEM formulation for the forward scattering problem. The FEM-BEM based scheme presented here has several advantages, including its straightforward implementation. Section 4 presents numerical results demonstrating the ability of our algorithm to reconstruct several test media.

2 Coupled FEM-BEM method

In this section we consider the forward problem with fixed incident direction $\widehat{\mathbf{d}}$ and given refractive index $m(\mathbf{x})$ for $\mathbf{x} \in B$. Following Kirsch and Monk [12], we introduce independent exterior and interior problems related to the forward problem (4)–(9) that are efficiently solved using the Nyström and finite element methods, respectively.

Exterior problem For given Robin boundary data λ defined on ∂B, the *exterior problem* is to compute the radiating solution w that satisfies

$$\Delta w(\mathbf{x}) + k^2 w(\mathbf{x}) = 0\,, \quad \mathbf{x} \in \mathbb{R}^2 \setminus B\,, \tag{10}$$

$$\frac{\partial w}{\partial \mathbf{n}}(\mathbf{x}) + ikw(\mathbf{x}) = \lambda(\mathbf{x})\,, \quad \mathbf{x} \in \partial B\,. \tag{11}$$

For this direct scattering problem, posed with a Robin boundary condition, it is efficient to use the surface integral representation

$$w(\mathbf{x}) = \int_{\partial B} \left[\frac{\partial G(\mathbf{x}, \mathbf{y})}{\partial \mathbf{n}(\mathbf{y})} w(\mathbf{y}) - G(\mathbf{x}, \mathbf{y}) \frac{\partial w(\mathbf{y})}{\partial \mathbf{n}} \right] ds(\mathbf{y})\,, \tag{12}$$

where $\mathbf{x} \in \mathbb{R}^2 \setminus B$ and $G(\mathbf{x}, \mathbf{y})$ is the free space Green's function for the two dimensional Helmholtz equation. Enforcing the boundary condition (11) and applying the jump relations [4, Thm. 3.1, p. 40] for the single- and double-layer potential operators yields the second kind integral equation

$$\begin{aligned} w(\mathbf{x}) - 2\int_{\partial B} \frac{\partial G(\mathbf{x}, \mathbf{y})}{\partial \mathbf{n}(\mathbf{y})} w(\mathbf{y})\, ds(\mathbf{y}) - 2ik \int_{\partial B} G(\mathbf{x}, \mathbf{y}) w(\mathbf{y})\, ds(\mathbf{y}) \\ = -2\int_{\partial B} G(\mathbf{x}, \mathbf{y}) \lambda(\mathbf{y})\, ds(\mathbf{y})\,, \quad \mathbf{x} \in \partial B\,. \end{aligned} \tag{13}$$

It is convenient to define $F_e \lambda = w$, where w is the solution of (13) on ∂B with given Robin boundary data λ. In our implementation we solve (13) using the high order Nyström scheme described by Colton and Kress [4, §3.5] with equally spaced quadrature points $\mathbf{x}_1, \ldots, \mathbf{x}_M$ on ∂B.

Interior problem For given Robin boundary data λ defined on ∂B, the *interior problem* is to compute the field v that satisfies

$$\Delta v(x) + k^2 m(x) v(x) = 0\,, \quad x \in B\,, \tag{14}$$

$$\frac{\partial v}{\partial n}(x) + ikv(x) = \lambda(x)\,, \quad x \in \partial B\,. \tag{15}$$

It is convenient to define $F_i\lambda = v|_{\partial B}$, where v is the solution of (14)–(15) with given Robin boundary data λ. Using a test function ϕ and Green's first identity leads to the weak equation

$$\int_B (\nabla v \cdot \nabla \phi - k^2 m v \phi)\, dv + ik \int_{\partial B} v\phi\, ds = \int_{\partial B} \lambda \phi\, ds\,. \tag{16}$$

We solve (16) using the finite element method, with piecewise linear functions defined on a triangular mesh for the interior region B, with (16) required to hold for all test functions ϕ in the standard nodal finite dimensional basis. The triangular mesh is chosen so that that the mesh points at the boundary include the quadature points $x_1, \ldots, x_M$ in the Nyström scheme described above.

Coupled FEM-BEM For Robin boundary data λ, the fields

$$u^s = F_e\lambda\,, \tag{17}$$

$$u^i = F_i(\lambda + Ru^{inc})\,, \tag{18}$$

satisfy (4)–(6), and the Robin trace of the total field (7) is continuous across ∂B. Here, for brevity, we denote by Ru the Robin trace of u,

$$(Ru)(x) = \frac{\partial u}{\partial n}(x) + iku(x)\,, \quad x \in \partial B\,.$$

To construct fields (17)–(18) that satisfy the transmission boundary conditions (8)–(9), we choose λ such that the Dirichlet trace of the total field is also continuous across ∂B, that is,

$$F_e\lambda + u^{inc} = F_i(\lambda + Ru^{inc})\,, \quad \text{on } \partial B. \tag{19}$$

It is convenient to parametrise ∂B using polar coordinates, and approximate the solution λ of (19) in the finite dimensional space spanned by $\{e^{in\theta} : n = -(N+1), \ldots, N\}$ using a Galerkin scheme. Here θ denotes the angle in polar coordinates. The Galerkin scheme is implemented with respect to the standard inner product on ∂B. In practice, integrals involved in the inner product are evaluated using the rectangle rule (which has high order accuracy on ∂B). In our implementation, we choose the quadrature points to coincide with the Nyström points $x_1, \ldots, x_M$. The operators F_e and F_i in our Galerkin scheme are evaluated numerically using the Nyström scheme or FEM, respectively.

Once λ is computed, the far field of u^s is given by [4, Eqn. (3.87), p. 75]

$$u^\infty(\hat{x}) = \frac{e^{i\pi/4}}{\sqrt{8\pi k}} \int_{\partial B} \left[\frac{\partial e^{-ik\hat{x}\cdot y}}{\partial n(y)} w(y) + ike^{-ik\hat{x}\cdot y} w(y) - e^{-ik\hat{x}\cdot y} \lambda(y) \right] ds(y) .$$

3 Inverse problem

In this section we describe our approach for reconstructing the refractive index m from given far field data. To simplify the description of our algorithm, we assume that the given far field data is for a single incident direction $\hat{d}$. Extension to the case of several incident directions is straightforward.

We assume that we are given far field data g_s for $s = 0, \ldots, S-1$ corresponding to observation directions

$$\hat{x}_s = \frac{2\pi s}{S}, \quad s = 0, \ldots, S-1 .$$

This far field data may include numerical or measurement errors, or other noise.

We seek an approximation to the refractive index m of the form

$$m_L(x) = \sum_{l=0}^{L} \sum_{j=0}^{l} m_{l,j} P_{l,j}(x), \quad x \in B , \tag{20}$$

where the Logan–Shepp polynomial

$$P_{l,j}(\boldsymbol{x}) = \frac{1}{\sqrt{\pi}} U_l(\boldsymbol{x} \cdot \boldsymbol{w}_{l,j}), \quad \text{for } j < l, l \in \mathbb{N} \text{ and } \boldsymbol{x} \in B, \tag{21}$$

where

$$\boldsymbol{w}_{l,j} = \left(\cos \frac{j\pi}{l+1}, \sin \frac{j\pi}{l+1} \right), \quad \text{for } j < l \text{ and } l \in \mathbb{N},$$

and U_l is the degree l Chebyshev polynomial of the second kind [1, Chap. 22]. The Logan–Shepp polynomials are orthogonal on the disk B and are used to approximate functions with high order accuracy. We show in our numerical experiments that $L = 15$ is sufficient to reconstruct the key features of the refractive index for a range of smooth and non-smooth inhomogeneous media.

We split the given far field data $g_0, \ldots, g_{S-1}$ into real and imaginary parts to construct $g = (g_0, \ldots, g_{2S-1})$ where

$$g_s = \begin{cases} \operatorname{Re} g_s, & \text{for } 0 \leqslant s \leqslant S-1, \\ \operatorname{Im} g_{s-S}, & \text{for } S \leqslant s \leqslant 2S-1. \end{cases} \tag{22}$$

We then reformulate the inverse medium problem as a finite dimensional real nonlinear problem of finding the vector $m = (m_{l,j})_{j<l\leqslant L}$ of spectral coefficients in the expansion (20), satisfying

$$F(m) = g, \tag{23}$$

where the nonlinear function $F : \mathbb{R}^{N_L} \to \mathbb{R}^{2S}$ is defined by $F(m) = f$, where the vector $f = (f_0, \ldots, f_{2S-1})$ for

$$f_s = \begin{cases} \operatorname{Re} u^\infty(\widehat{\boldsymbol{x}}_s; m_L), & \text{for } 0 \leqslant s \leqslant S-1, \\ \operatorname{Im} u^\infty(\widehat{\boldsymbol{x}}_{s-S}; m_L), & \text{for } S \leqslant s \leqslant 2S-1, \end{cases} \tag{24}$$

and $u^\infty(\cdot; m_L)$ denotes the numerical approximation to the far field of the scatterer with refractive index m_L, computed using the coupled FEM-BEM scheme in the previous section. Here $N_L = (L+1)(L+2)/2$ is the dimension of the ansatz space for the reconstructed refractive index.

We solve the ill–posed nonlinear problem (23) using the Levenburg–Marquardt iteration [8, 4, 11]. Due to the low dimension of the ansatz space, it is feasible to assemble a numerical approximation to the derivative of the nonlinear operator F using forward differences. In particular, although a forward problem with a different inhomogeneous medium must be solved numerically for each column of the derivative, the BEM part is independent of the medium and the FEM part is cheap, provided the wavelength is not too small. In our implementation we take advantage of the independence of the interior problems for each column of the derivative by computing the columns in parallel.

In our numerical experiments we found it useful to decompose the complex far field values into real and imaginary parts in (22) and (24), because (23) is then solved in real arithmetic, which naturally enforces the physically appropriate condition that the refractive index is real valued.

4 Numerical experiments

In this section we demonstrate our algorithm by reconstructing the refractive index function of several test inhomogeneous media. In particular, our test problems are as follows.

- **Bowl**: the inhomogeneous region is the off-centre disk of radius $1/2$ centred on $\mathbf{c} = (0.3, 0.3)$. The continuous refractive index function is

$$m(\mathbf{x}) = \begin{cases} 2 - 4|\mathbf{x} - \mathbf{c}|^2, & \text{for } |\mathbf{x} - \mathbf{c}| < 1/2, \\ 1, & \text{otherwise.} \end{cases}$$

- **Ellipse**: the inhomogeneous region is contained inside an ellipse. The discontinous refractive index function is

$$m(\mathbf{x}) = \begin{cases} 1.21, & \text{for } x_1^2/4^2 + x_2^2/5^2 \leqslant 1/10^2, \\ 1, & \text{otherwise.} \end{cases}$$

- **Three disks**: the inhomogeneous region comprises three disks of radius $1/4$ and centres $\mathbf{c}_1 = (0.4, 0)$, $\mathbf{c}_2 = (-0.2, 0.346)$ and $\mathbf{c}_3 = (0.2, -0.346)$. The discontinous refractive index function is

$$m(\mathbf{x}) = \begin{cases} 1.21, & \text{for } |\mathbf{x} - \mathbf{c}_1| < 1/4\,, \\ 1.21, & \text{for } |\mathbf{x} - \mathbf{c}_2| < 1/4\,, \\ 1.44, & \text{for } |\mathbf{x} - \mathbf{c}_3| < 1/4\,, \\ 1, & \text{otherwise.} \end{cases}$$

For the bowl problem we use our coupled FEM-BEM forward solver to compute the far field corresponding to the inhomogeneous medium, and we generate our reference data by adding Gaussian noise. For the discontinuous ellipse and three disks media we generate reference data using solvers that are independent of our coupled FEM-BEM code. In particular, for the three disks problem the reference data is generated using a multiple scattering version of the Mie series. For the discontinous ellipse problem, the reference data is generated using a surface integral equation formulation [3] that we solve using a high order Nyström scheme [4, §3.5]. Thus none of our numerical experiments are subject to the so called *inverse crime* of using data that is generated directly by the forward solver used for the inversion.

Table 1 demonstrates the small number of degrees of freedom required to approximate the refractive indices of our test media using the Logan–Shepp expansion (20). In particular, we tabulate the relative L_2 error in the discrete orthogonal projection of the refractive index. In practice, the L_2 norm is approximated using a Gauss-rectangle rule with more than $20\,000$ points in the disk. The slow convergence observed in Table 1 is due to the low regularity of the refractive index functions (the refractive indices of the ellipse and three disks media are discontinuous).

Motivated by the results in Table 1, we apply our algorithm to reconstruct the three test media from far field data, using polynomials of degree $L = 15$ in the Logan–Shepp expansion (20). In Table 2 we tabulate the relative L_2 error in the reconstructed refractive index $m(\mathbf{x})$ in the unit disk for each medium, and

Table 1: Relative L_2 error of the discrete orthogonal projection of the refractive index against number of degrees of freedom (dof).

degree L	dof N_L	error bowl	error ellipse	error three disks
5	21	6.6%	4.3%	9.1%
10	66	2.5%	3.3%	5.5%
15	136	1.4%	2.6%	5.3%

Table 2: Relative L_2 error of the reconstructed refractive index function $m(x)$ in the unit disk for Logan–Shepp polynomial degree $L = 15$.

medium	noise σ	error $k = \pi$	error $k = 2\pi$
bowl	0	0.72%	3.4%
	1×10^{-2}	8.1%	15%
	5×10^{-2}	16%	24%
ellipse	0	9.4%	8.9%
three disks	0	18%	13%

for wavenumbers $k = \pi$ and $k = 2\pi$. At these wavenumbers, the diameter of the unit disk is one and two times the incident wavelength, respectively. The CPU times for the bowl problem are 3.2 hours for the $k = \pi$ case and 12.3 hours for the $k = 2\pi$ case, using Matlab with the parallel computing toolbox, running on a desktop machine with a quad-core 2.8 GHz Intel Core i7 processor. The CPU times for the ellipse and three disks problems are similar. The reference data is obtained by adding Gaussian noise to simulated far field values at 32 equally spaced points on the unit circle for each of the six incident directions

$$\widehat{d}_j = \frac{2\pi j}{6}, \quad j = 0, \ldots, 5.$$

In particular, the reference data g_s for $s = 0, \ldots, S-1$ is obtained by adding noise $x_s + iy_s$ to the simulated data where x_s and y_s for $s = 0, \ldots, S-1$

Figure 1: Reconstruction of the refractive index $m(\mathbf{x})$ in the unit disk for the bowl test problem with noise parameter $\sigma = 5 \times 10^{-2}$, polynomial degree $L = 15$ and six incident directions. The wavenumber is $k = 2\pi$ and the diameter of the domain equals twice the incident wavelength.

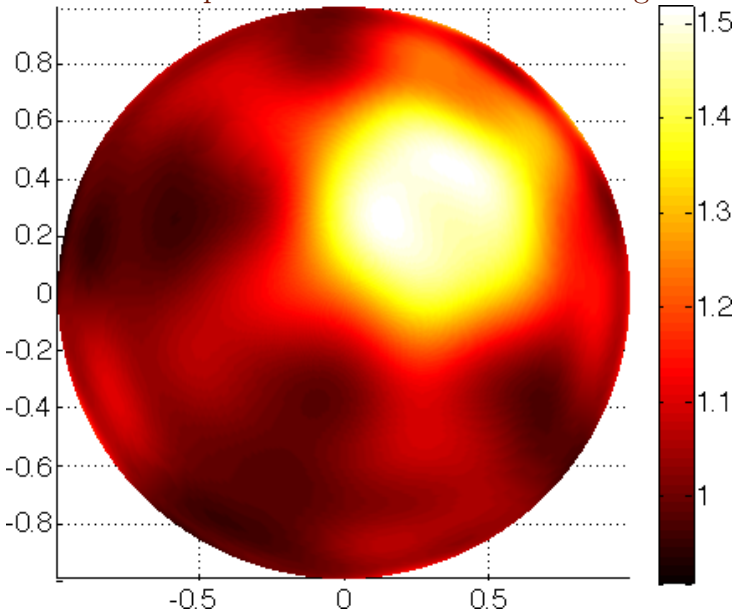

are independent samples of the Gaussian distribution with zero mean and variance σ^2.

In Figures 1 and 2 we visualise the reconstructed refractive index $m(\mathbf{x})$ for our most difficult test problems. In both cases the Logan–Shepp polynomial degree is $L = 15$ and the incident wavenumber is $k = 2\pi$. The relative L_2 error in the reconstruction of the bowl (with large noise parameter) is 24% (Figure 1). The relative L_2 error in the reconstruction of the three disks is 13% (Figure 2). We do not expect very small errors for these problems, due to the low regularity of the refractive index, but we get excellent reconstruction of the key features of the media such as the locations, sizes and refractive indices of any inhomogeneities.

Figure 2: Reconstruction of the refractive index $m(x)$ in the unit disk for the three disks test problem with polynomial degree $L = 15$ and six incident directions. The wavenumber is $k = 2\pi$ and the diameter of the domain equals twice the incident wavelength.

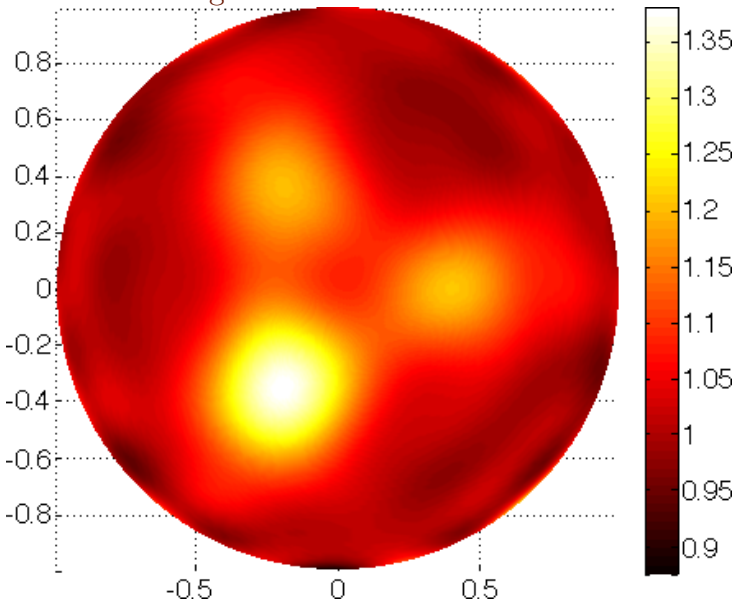

5 Conclusions

We demonstrated the effectiveness of our coupled FEM-BEM based scheme for reconstructing the refractive index of an inhomogeneous two dimensional medium from far field data. The FEM-BEM based scheme presented here has several advantages, including its straightforward implementation. Additionally, the FEM-BEM based scheme presented here is readily adapted to non-circular domains bounding the inhomogeneity, and indeed, to more complex geometries such as domains with inclusions. In future work we will extend our scheme to reconstruct unknown media surrounding a perfectly conducting inclusion.

References

[1] M. Abramowitz and I. A. Stegun, editors. *Handbook of Mathematical Functions*. National Bureau of Standards, 1964. doi:10.1119/1.1972842. C171

[2] K. Atkinson, D. Chien, and O. Hansen. A spectral method for elliptic equations: the Dirichlet problem. *Adv. Comput. Math.*, 33:69–1891, 2014. doi:10.1007/s10444-009-9125-8. C167

[3] A. Barnett and L. Greengard. A new integral representation for quasi-periodic fields and its application to two-dimensional band structure calculations. *J. Comput. Phys.*, 229:6898–6914, 2010. doi:10.1016/j.jcp.2010.05.029. C173

[4] D. Colton and R. Kress. *Inverse Acoustic and Electromagnetic Scattering Theory*. Springer, 2012. doi:10.1007/978-1-4614-4942-3. C165, C167, C168, C170, C172, C173

[5] S. Gutman and M. Klibanov. Regularized quasi-Newton method for inverse scattering problems. *Math. Comput. Modelling*, 18:5–31, 1993. doi:10.1016/0895-7177(93)90076-B. C167

[6] S. Gutman and M. Klibanov. Iterative method for multi-dimensional inverse scattering problems at fixed frequencies. *Inverse Problems*, 10:573–599, 1994. doi:10.1088/0266-5611/10/3/006. C167

[7] S. Gutman and M. Klibanov. Two versions of quasi-Newton method for multidimensional inverse scattering problem. *J. Comput. Acoust.*, 1:197–228, 1993. doi:10.1142/S0218396X93000123. C167

[8] M. Hanke. A regularizing Levenburg-Marquardt scheme, with applications to inverse groundwater filtration problems. *Inverse Problems*, 13:79–95, 1997. doi:10.1088/0266-5611/13/1/007. C167, C172

[9] T. Hohage. On the numerical solution of a three-dimensional inverse medium scattering problem. *Inverse Problems*, 17:1743–1763, 2001. doi:10.1088/0266-5611/17/6/314. C167

[10] T. Hohage. Fast numerical solution of the electromagnetic medium scattering problem and applications to the inverse problem. *J. Comput Phys.*, 214:224–238, 2006. doi:10.1016/j.jcp.2005.09.025. C167

[11] A. Kirsch. *An Introduction to the Mathematical Theory of Inverse Problems*. Springer, 2011. doi:10.1007/978-1-4419-8474-6. C167, C172

[12] A. Kirsch and P. Monk. An analysis of the coupling of finite-element and Nyström methods in acoustic scattering. *IMA J. Numer. Anal*, 14:523–544, 1994. doi:10.1093/imanum/14.4.523. C166, C168

[13] B. F. Logan and L. A. Shepp. Optimal reconstruction of a function from its projections. *Duke Math. J.*, 42:645–659, 1975. doi:10.1215/S0012-7094-75-04256-8. C166

Author addresses

1. **S. Bagheri**, Department of Mathematics, Macquarie University, Sydney, NSW 2109, Australia.
mailto:sherwin.bagheri@mq.edu.au

2. **S. C. Hawkins**, Department of Mathematics, Macquarie University, Sydney, NSW 2109, Australia.
mailto:stuart.hawkins@mq.edu.au